Intracollisional interference in resonant collisions of Na Rydberg atoms

D. S. Thomson, R. C. Stoneman,* and T. F. Gallagher
Department of Physics, University of Virginia, Charlottesville, Virginia 22901
(Received 6 October 1988)

The theory of resonant dipole-dipole energy transfer in an electric field **E** indicates substantial differences between the collision velocities **v**||**E** and **v**⊥**E**. For **v**||**E** the cross section vanishes at exact resonance due to a destructive interference in the transition amplitude, producing a double-peaked line shape. The presence of the permanent dipole moments in the field produces slight shifts and asymmetries of the collisional resonance line shapes. A high-resolution experimental study of the cases **v**||**E** and **v**⊥**E** indicates that the theoretical predictions are correct and further allows the resolution of the spin-orbit structure in the resonant collisions.

I. INTRODUCTION

Resonant dipole-dipole collisional energy transfer between Rydberg atoms, first observed by Safinya *et al.*,[1] occurs with large collision cross sections and long interaction times. As an example, the cross section for two Na $n=20$ atoms resonantly transferring energy in a thermal collision is $\sim 10^8$ Å^2, and the collision time is ~ 1 ns.[1] Such large cross sections and long interaction times afford some unique opportunities to investigate relatively fine details of collisional processes. One example is radiative collisions, in which the stimulated emission of one or several microwave photons occurs during the collision.[2,3]

To date all the measurements of resonant collisions in Rydberg atoms have been done using a relatively small electric field to tune the energy levels through the collisional resonance. In addition to providing the energy resonance, the tuning field introduces significant and interesting alignment effects. In the presence of the field there are two natural directions in the problem, those of the field **E** and the collision velocity **v**. Furthermore, the presence of the field destroys the parity of the participating atomic states with the result that they have substantial aligned permanant electric dipole moments, which can play a role in a dipole-dipole collision process.

It is our purpose here to examine these alignment issues, theoretically and experimentally. Specifically we have studied the effect of the relative orientations of **v** and **E** on the resonant collision process $ns+ns\rightarrow np+(n+1)p$ in Na, which is tuned into resonance with an electric field. As we shall see, a theory based on the resonant dipole-dipole interaction predicts that the cross section vanishes for **v**||**E** at resonance, but is nonzero near resonance, leading to a double-peaked resonance line shape. The origin of this line shape is an intracollisional interference effect analogous to the interference in the Ramsey method of separated oscillatory fields.[4] We note that intercollisional interference effects, observed in collision-induced absorption, have also been interpreted in terms of the Ramsey method.[5] When the permanent dipole moments are omitted the resonance is symmetric, but when they are included an asymmetry appears. For **v**⊥**E** a single-peaked, nearly Lorentzian resonance is predicted. Again the inclusion of the permanent moments introduces a slight asymmetry into the line shape.

To investigate these predictions experimentally has required substantial refinement of the experimental techniques. First, instrumental broadening of the resonances was reduced by improved field homogeneity, allowing the spin-orbit splitting of the p states to be observed for the first time as well. Second, several variations in the geometry of the apparatus were used to allow the study of **v**||**E** and **v**⊥**E** collisions.

II. THEORY

The large cross sections previously measured for the collision process being discussed, as well as the large electric dipole moments characteristic of Rydberg atoms, suggest that an appropriate model for these collisions is a long-range dipole-dipole interaction. Just such a model was used in an approximate way by Safinya *et al.*[1] and later more exactly by Fiordilino *et al.*[6] to analyze the data of the first study[1] of these resonant collisions in Na. Although the use of this model was successful in many respects, an analytic solution can only be found in a restricted set of circumstances. In particular, the transition probability can only be found for the case in which the system is on resonance and in which the permanent dipole moments are ignored. Under these conditions the transition probability vanishes for **v**||**E**, which we show by deriving an explicit form for the transition probability in terms of the angle between **E** and **v**. To show the line shapes of the collisional resonances we present the results of numerical calculations of transition probabilities as a function of the detuning from exact resonance. These calculations are done both with and without the permanent dipole moments to assess their effect on the collision process.

A. Theoretical model

Consider an atomic collision as viewed from the rest frame of one of the atoms. Let **R** be the distance between atoms, and **v** be the velocity of the moving atom (or the relative velocity in the laboratory frame of reference). If

we make the assumption that the collision does not deflect the moving atom, then $\mathbf{R}=\mathbf{b}+\mathbf{v}t$, where $\mathbf{b}$ is the impact parameter. It is most convenient to describe the geometry of such a collision in terms of two angles, θ and ϕ, shown in Fig. 1. We define θ as the polar angle of $\mathbf{b}$ with respect to the static electric field, which is taken as the z axis. The x and y axes are chosen so that $\mathbf{b}$ lies in the x-z plane, ϕ is then taken as the negative of the azimuthal angle of $\mathbf{v}$ in a coordinate system in which $\mathbf{b}$ lies along the z' axis.

The long interaction times observed for these collisions imply that the interaction occurs at long range, and we assume that the interaction potential can be adequately described by the electric dipole-dipole term

$$V=\frac{\mathbf{D}(1)\cdot\mathbf{D}(2)}{R^3}-3\frac{[\mathbf{D}(1)\cdot\mathbf{R}][\mathbf{D}(2)\cdot\mathbf{R}]}{R^5}\ , \tag{1}$$

with $\mathbf{D}(1)$ and $\mathbf{D}(2)$ the dipole moments. The Hamiltonian for the system is

$$H(t)=H_{01}+H_{02}+V(\mathbf{R},\mathbf{D}(1),\mathbf{D}(2),t)\ , \tag{2}$$

where H_{01} and H_{02} are the Hamiltonians of the individual atoms in the electric field with eigenstates $U_{nlm}(1)$ and $U_{nlm}(2)$ and energy eigenvalues $E_{nlm}(1)$ and $E_{nlm}(2)$. If we define the product states

$$\psi_i=U_{ns0}(1)U_{ns0}(2)$$

and

$$\psi_f=\frac{1}{\sqrt{2}}[U_{npm}(1)U_{(n-1)pm}(2)+U_{(n-1)pm}(1)U_{npm}(2)]$$

and assume a general solution of the form

$$\Psi(t)=C_i(t)\psi_i+C_f(t)\psi_f\ ,$$

then applying the Schrödinger equation yields the pair of equations

$$i\hbar\dot{C}_i=(2E_{ns0}+V_{ii})C_i+V_{if}C_f\ , \tag{3a}$$

$$i\hbar\dot{C}_f=V_{fi}C_i+(\varepsilon+V_{ff})C_f\ . \tag{3b}$$

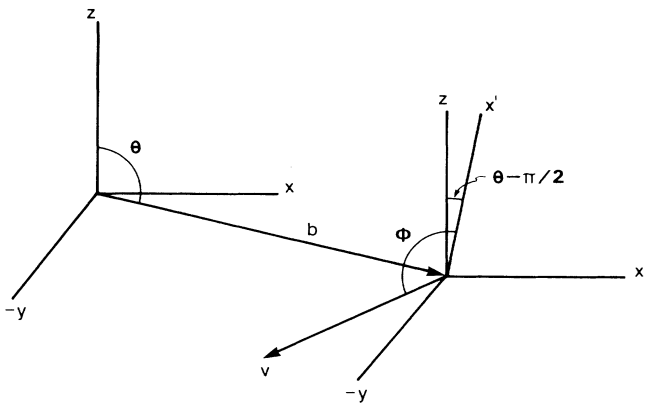

FIG. 1. Geometry of the experiment in the rest frame of one atom showing the definitions of θ and ϕ. Components of $\vec{R}=\vec{b}+\vec{v}t$ are $x=-vt\cos\theta\cos\phi+b\sin\theta$, $y=vt\sin\phi$, and $z=vt\sin\theta\cos\phi+b\cos\theta$.

E_{ns0} is defined as the zero of energy, and $\varepsilon=E_{(n-1)pm}+E_{npm}$ is the detuning energy. The above coupled equations can be solved analytically at resonance ($\varepsilon=0$) assuming that the matrix elements of the dipole-dipole potential satisfy $V_{if}=V_{fi}$ and $V_{ii}=V_{ff}=0$. With these assumptions and the additional condition that at $t=-\infty$, $C_i=1$ and $C_f=0$, we find the solution

$$C_i(t)=\cos\left[\int_{-\infty}^{t}V_{if}(t')dt'\right]\ ,$$
$$C_f(t)=\sin\left[\int_{-\infty}^{t}V_{if}(t')dt'\right]\ . \tag{4}$$

The probability of making a transition is therefore

$$P(\infty)=|C_f(\infty)|^2=\sin^2\left[\int_{-\infty}^{\infty}V_{if}(t')dt'\right]\ . \tag{5}$$

In the field the $|m|=0$ and 1 states of the two p levels are separated in energy, leading to the observation of four collisional resonances in previous experiments. The resonances were labeled (m_1,m_2) where m_1 and m_2 are the $|m|$ values of the upper and lower p state, respectively. Following this convention we now consider the (0,0) transition, for which

$$\int_{-\infty}^{\infty}V_{if}(t')dt'=2\frac{D(n,0;n,1)D(n,0,n-1,1)}{vb^2}(1-2\cos^2\theta-\sin^2\theta\cos^2\phi)\ . \tag{6}$$

Here $D(n,l,n'l')$ are the integrated interaction dipole matrix elements. It is obvious from Eqs. (5) and (6) that for the choice of angles $\theta=\pi/2$, $\phi=0$, the transition probability vanishes, whereas for $\theta=0$ it is nonzero for most values of v and b. Thus this solution predicts that for the $\varepsilon=0$ case, the (0,0) resonance observed when the static electric field is perpendicular to $\mathbf{v}$ will no longer be observed if the electric field and the relative velocities are made parallel to each other.

B. Numerical solutions

Reviewing Eqs. (3a) and (3b) and the restrictions which allowed them to be solved analytically, the first restriction to come under further scrutiny is that V_{ii} and V_{ff} are vanishingly small. Although this is obviously true in zero field, where l is a good quantum number, it is no longer true at the static electric fields at which the experiment was carried out. At the fields required for resonance, the nominal p states have 10–15% d-character admixtures. From the calculated energy levels of Na in static fields the $17p$-state dipole moment is found to be $\mu_{\rm perm}=182.3$ a.u. When this is compared to the interaction dipole moment $\mu_{\rm int}\simeq 0.6n^{*2}=156.4$ a.u., it seems clear that the permanent dipole moments must be included to find an accurate solution. The second restriction which we must consider is calculating the cross section only at exact resonance. Although calculating the cross

section at the exact resonance often gives a good indication of the cross section averaged over the resonance line shape, this assumption is less likely to be good when the cross section vanishes at exact resonance. Consequently, finding a solution which includes the detuning is desirable since calculations of the line shape are then possible.

With the inclusion of the permanent dipole terms and the detuning energy, there is no known analytical solution to Eqs. (3a) and (3b), and a numerical integration technique must be used to calculate transition probabilities. The Taylor expansion method,[7] carried to third order, can be shown to be sufficiently accurate by calculation transition probabilities for the case in which $V_{ii}=0$, $V_{ff}=0$ and $\varepsilon=0$, and comparing these calculations to the analytic solution. This was carried out for the $17s+17s\rightarrow 17p+16p$ (0,0) transition using an impact parameter of ~ 0.5 μm and an integration step size of 10 ps. For the case of $\mathbf{v}\perp\mathbf{E}$, the analytic solution yields a value of $P=0.007\,057\,0$, whereas the numerical value is $P=0.007\,057\,6$. For $\mathbf{v}\parallel\mathbf{E}$, the analytic values is $P=0.0$, and the calculated value is less than 10^{-9}.

Once the accuracy of the numerical integration is verified, calculations of the transition probability which include the effects of the permanent dipole moments and the detuning energy can be carried out. In doing this, the values $\mu_{16p}=113.3$, $\mu_{17s}=-16.5$, and $\mu_{17p}=182.3$ are used for the permanent dipole moments, and $\mu_{\rm int}=156.4$ is used for the interaction dipole moment. Figure 2 shows the results of these calculations for two cases. In Fig. 2(a) the electric field and collisional velocity are parallel, and in Fig. 2(b) the electric field and collisional velocity are perpendicular to each other. As shown in Fig. 2, the calculations have been done with the permanent electric dipole moments both included and omitted. The collisional velocity used in the calculations is $v_0=1.6\times 10^{-4}$ a.u. (3.5×10^4 cm/s), and the impact parameter is approximately $10^4 a_0$, where a_0 is the Bohr radius, 0.53 Å. Also, calculations such as those shown in Fig. 2(b) in which $\mathbf{v}\perp\mathbf{E}$ have been carried out for $\theta=0$, $\phi=\pi/2$, and are not averages over θ as is the case experimentally. Although the line shape does vary with θ, the features being discussed here are not significantly affected by this variation. The first observation to be made regarding these calculations is that the transition probability does indeed vanish at exact resonance when $\mathbf{v}\parallel\mathbf{E}$, regardless of whether or not the permanent dipole moments are included in the solution. This is in agreement with the analytic solution, but the more complete numerical solution makes it obvious that the transition probability does not identically vanish for the $\mathbf{v}\parallel\mathbf{E}$, but has a double-peaked structure as shown in Fig. 2(a).

A second conclusion which can be drawn from the calculations is that the interaction of the permanent dipole moments is responsible for both a shift and an asymmetry in the resonances. This can be seen in Fig. 2, in which the dashed lines are the calculations of the line shapes when the permanent dipole moments are ignored. Inclusion of the permanent dipole moments results in a definite asymmetry and a shift in resonance as shown by the solid lines. The relatively small magnitude of these effects combined with the effects of averaging over impact parameter and collision velocity makes them difficult but not impossible to observe.

The origin of the double-peaked line shape of Fig. 2(a) can be understood in the terms of radio frequency resonance. In fact, the line shape has roughly the same form and origin as the Ramsey separated oscillatory field pattern when there is a 180° phase shift between the two oscillatory fields.[4] We begin by examining a plot of the interaction potential, $V(r)$ as a function of r. As shown by Fig. 3, for $\mathbf{E}\parallel\mathbf{v}$ the interaction parameter changes sign twice during the collision so that $\int_{-\infty}^{\infty} V(r)dt=0$. This is approximately equivalent to doing a radio frequency experiment in which the phase of the rf field is twice changed by 180°. At resonance, the contributions to the

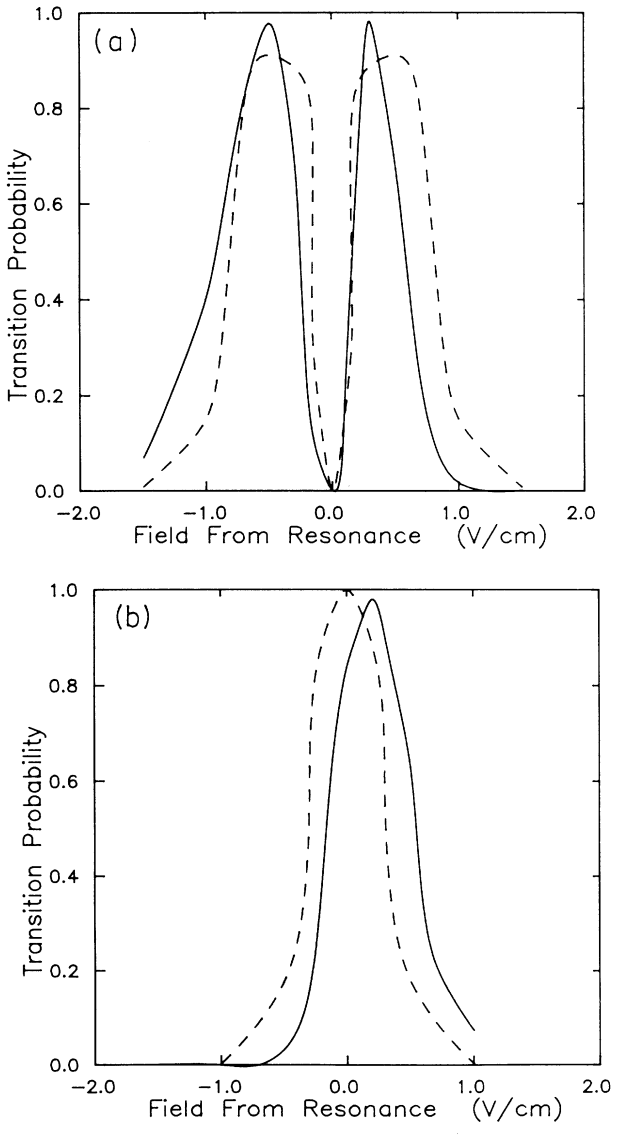

FIG. 2. Calculations of the transition probability for the $17s+17s\rightarrow 17p+16p$, (0,0) transition for (a) $\mathbf{v}\parallel\mathbf{E}$, and (b) $\mathbf{v}\perp\mathbf{E}$. Solid lines are for calculations which include the effects of the permanent dipole moments; dashed lines indicate that the permanent dipole moments have been neglected.

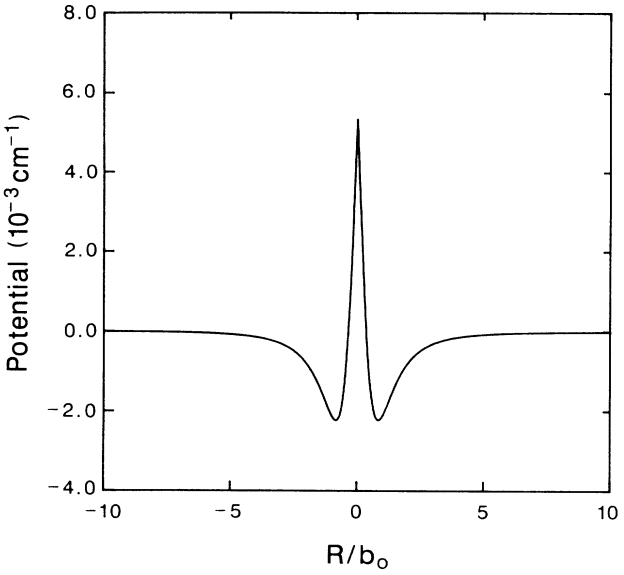

FIG. 3. Dipole-dipole interaction potential for the case in which $\mathbf{v}\|\mathbf{E}$. The abscissa is in units of R/b_0 where b_0 is defined by $\sigma = 2.3\pi b_0^2$ (Ref. 1) and is taken as $10^4 a_0$.

transition amplitude from $V(r)<0$ cancel those from $V(r)>0$ so that, integrated over the whole collision, the transition probability vanishes. Off resonance, however, the cancellation is not complete.

The difference between on and off resonance can be seen graphically if we use the rotating coordinate system of the two-level, spin-$\frac{1}{2}$ magnetic resonance problem. Imagine that we have a magnetic moment μ in a static magnetic field B_z in the z direction. The magnetic moment precesses about the static field at the Larmor frequency μB_z, which is also the frequency corresponding to the energy splitting between spin up and spin down. Now imagine that we apply a magnetic field B_{xy} which rotates in the x-y plane. If the field rotates at the Larmor frequency, then in its rotating coordinate system the magnetic moment does not appear to rotate about the z axis. Effectively, by transforming the problem to the rotating coordinate system we have transformed the static magnetic field B_z to zero. In the rotating frame the magnetic moment sees only the static field B_{xy} and precesses about it at the frequency μB_{xy}. A magnetic moment initially pointing up can precess about the horizontal B_{xy} to point down, corresponding to 100% transition probability from spin up to spin down. The direction that the field B_{xy} points in the x-y plane, which is determined by the phase of the microwaves, is clearly insignificant in this case. If the horizontal magnetic field does not rotate at the Larmor, or resonance, frequency, in the rotating frame, B_z is not transformed to zero and the net magnetic field is not in the x-y plane, thus the precession is about an axis which lies out of the x-y plane.

Now let us consider the analogue of the resonant collision interaction depicted in Fig. 3. First we consider the case of exact resonance. A magnetic moment which initially has its spin pointing up is exposed to a succession of three exactly resonant rf pulses. To be specific, the rf-field changes sign, i.e., there is a 180° phase shift, between the rf pulses, and the second pulse is twice as long as the first and third. Since the direction in which B_{xy} points is determined by the rf phase, during the second pulse B_{xy} points in the direction opposite to its direction in the first and third pulses and the sense of the precession is similarly reversed. In Fig. 4(a) we show the precession of the magnetic moment produced by the three rf pulses described above. We have taken B_{xy} to lie along the positive y axis for the first and third pulses and along the negative y axis for the second. As shown by Fig. 4(a) the precession of the magnetic moment occurs entirely in the y-z

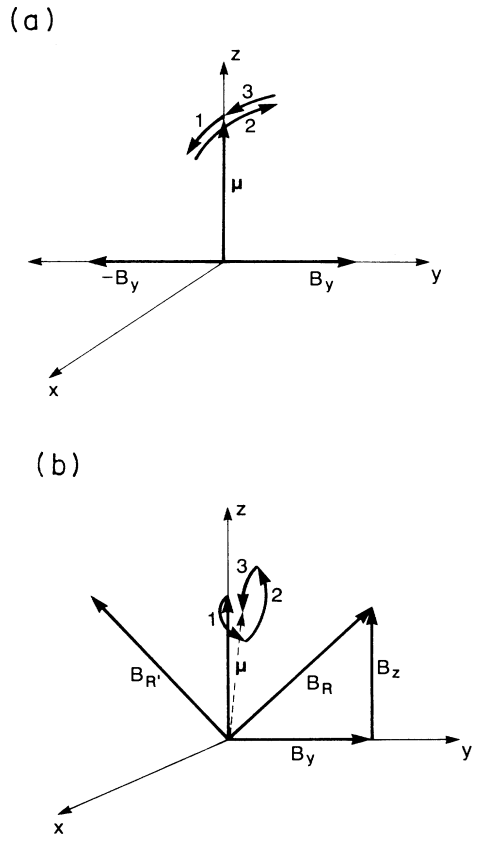

FIG. 4. Precession of the magnetic moment in the rotating coordinate system when three rf pulses are applied, the second being twice as long as the first and third and being phase shifted by 180° from them. The rf magnetic field is $\mathbf{B}_y$ in the first and third pulses and $-\mathbf{B}_y$ in the second. At resonance (a) $|B_y|$ is the only magnetic field and the magnetic moment μ, initially pointing in the z direction, precesses in the x-z plane with the precession in the second pulse canceling the precession in the first and third pulses. Off resonance (b) there is a residual magnetic field $\mathbf{B}_z$ in the z direction leading to the resultant fields $\mathbf{B}_R$ in the first and third rf pulses and $\mathbf{B}_{R'}$ in the second. Since $\mathbf{B}_R \neq \mathbf{B}_{R'}$ the precessions of the magnetic moment are not in the same plane and do not cancel, as shown by the numbered arcs. The final orientation of the moment is shown by the broken line. It is not along the z axis, corresponding to a nonzero transition probability from spin up to spin down.

plane and the precession during the second pulse precisely cancels the precession in the first and third pulses.

Now consider the case in which the rotating field is slightly off resonance. In this case B_z is nonzero in the rotating frame, and the resultant field B_R does not lie in the x-y plane. This is shown in Fig. 4(b) for a detuning from resonance equal to μB_{xy}. Most important, as shown in Fig. 4(b), when the rf phase is reversed in the second pulse the resultant field $B_{R'}$ is not in the direction opposite to that of the resultant field during the first and third pulses. Thus the precession of the magnetic moment during the second pulse is in a different plane from that in the first and third pulses, and the precession during the second pulse cannot cancel the precession of the first and third pulses. The off-resonant precession of the magnetic moment is shown in Fig. 4(b), which shows that the magnetic moment does not precess back to its starting point. Correspondingly, there is a nonzero probability of making the transition from spin up to spin down.

In our resonant collision experiments the dipole-dipole interaction $V(r)$, given by Eq. (1), corresponds to μB_{xy}. The sign changes in $V(r)$ correspond to 180° phase shifts of the rf. In our collisional resonances the resonance occurs when the $nsns$ and $np(n+1)p$ states are degenerate, and the detuning from the collisional $ns+ns \rightarrow np+(n-1)p$ resonance has the same effect as the detuning in the magnetic resonance case.

To calculate a cross section we must integrate the transition probability over impact parameter and average over the thermal distribution of collision velocities. To carry out these calculations over such a large parameter space using the Taylor expansion method is prohibitively time consuming. However, much can be learned by investigating the dependence of the line shape on each of these parameters independently. When integrating over impact parameter, we have used the more efficient method of Fiordilino *et al.*[6] Their method does, however, neglect the permanent moments, but as we have already seen this should not have a major effect. The results of these calculations are shown in Figs. 5(a) and 5(b) for $\mathbf{v}\|\mathbf{E}$ and $\mathbf{v}\perp\mathbf{E}$ respectively. We note that for $\mathbf{v}\|\mathbf{E}$, the zero in the transition probability seen in Fig. 2(a) survives, mainly because altering the impact parameter does

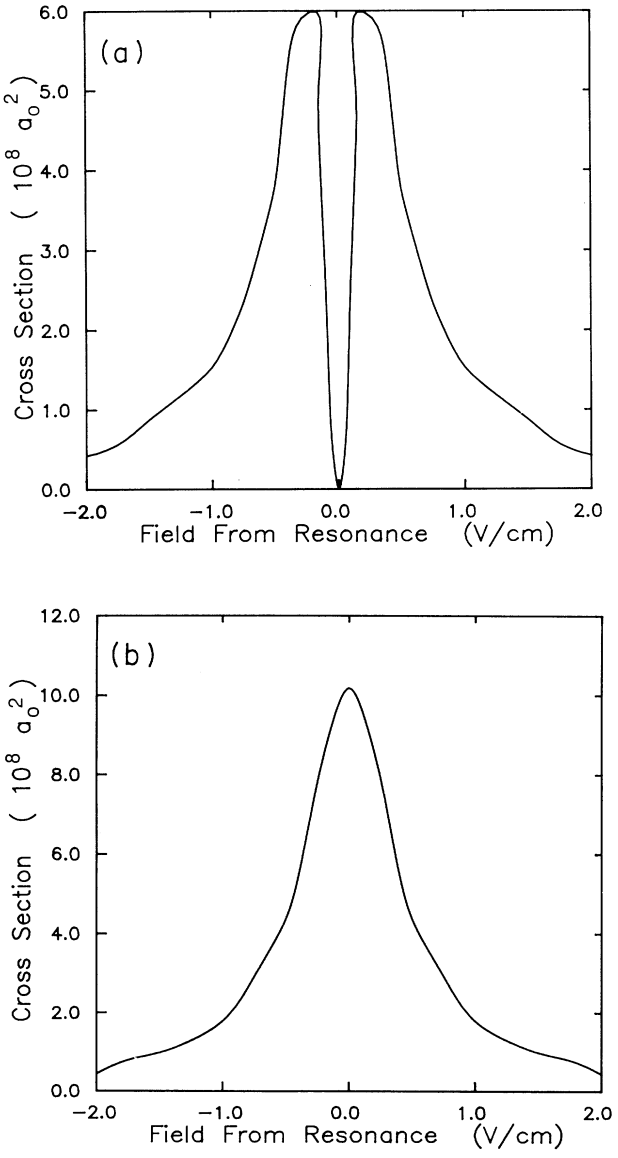

FIG. 5. Calculations of the collision cross section for the 17s (0,0) transition integrated over impact parameter for (a) $\mathbf{v}\|\mathbf{E}$ and (b) $\mathbf{v}\perp\mathbf{E}$. These calculations were carried out for one value of collision velocity using the method of Fiordilino *et al.* (Ref. 6) which ignores the permanent electric dipole moments.

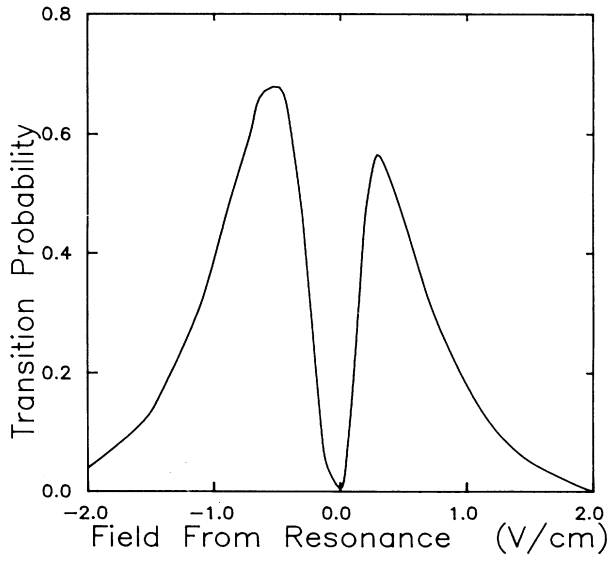

FIG. 6. Calculation of the 17s (0,0) transition probability for $\mathbf{v}\|\mathbf{E}$ averaged over velocity using the Taylor expansion method with impact parameter $b_0=10^4 a_0$. The inclusion of the permanent electric dipole moments in the solution causes the resonance to be shifted to a lower field, and averaging over velocity results in the low-field peak being taller than the high-field peak.

not change the symmetry of the line, only its width. In any event the peak cross sections for $\mathbf{v}\|\mathbf{E}$ and $\mathbf{v}\perp\mathbf{E}$ are roughly the same, $0.60\times10^{8}a_0^2$ and $1.0\times10^{9}a_0^2$, respectively. Examining Fig. 5, it is evident that the central zero is broad enough that one can imagine detecting it in an experiment. Also, the integrated cross sections, in the units of Fig. 5, are $8.3\times10^{8}a_0^2$ V/cm and $1.2\times10^{9}a_0^2$ V/cm, so in a low-resolution experiment the observed cross sections should be nearly the same.

It was found that averaging over collision velocity had an interesting effect on the asymmetry of the line shape. Since the asymmetry is due to the inclusion of the permanent dipole moments, it is necessary to use the Taylor expansion method to do this calculation. As can be seen in Fig. 2(a), both peaks in the double-peak structure have nearly the same magnitude when calculated for the velocity of 1.6×10^{-4} a.u. Similar calculations using the same impact parameter but different velocities show that as the velocity increases, the resonance shifts more to a lower field, so that the left peak broadens out and the right peak becomes narrower. Neither peak, however, becomes taller than the other. It is only when the line shapes for these different velocities are averaged together that the left peak, in addition to being broader than the right, is also taller, as shown by Fig. 6.

III. EXPERIMENTAL METHOD

In the experiment, metallic Na is heated to produce a thermal atomic beam. As Fig. 7 shows, this atomic beam passes through a collimator and into the interaction region. Here it intersects perpendicularly two collinear laser beams which excite the atoms to the *ns* Rydberg state in a two-step process. In the first step, a yellow dye laser beam is tuned to 5890 Å and excites the 3*s*-3*p* transition. The second dye laser is tuned to the 3*p*-*ns* transition (with $n=17$–24) at ~4140 Å. The two dye lasers are pumped by the second and third harmonics, respectively, of a pulsed yttrium aluminum garnet Nd:(YAG) laser, which has a repetition rate of 20 Hz.

Both the laser excitations and the subsequent collisions take place within a uniform static electric field. This field is created by a pair of parallel plates separated by 1.592(2) cm and is homogeneous to 1 part in 10^4. The electric field varies from 50 to 600 V/cm, depending on the state being studied, and is swept through the region of the resonances over ~1000 laser pulses.

Approximately 1 μs after the laser excitation, a high-voltage ionizing pulse is applied to one of the electric field plates. This pulse has a rise time of about 0.5 μs and produces a field pulse of amplitude as high as 6000 V/cm. As has been described elsewhere,[8] such an ionizing pulse leads to temporally resolved field ionization signals from different Rydberg states, and the variable rise time can be adjusted to optimize the resolution of the particular states being studied. For this experiment, the pulse is adjusted so that the *np* state and the *ns* state are well resolved, and a resonance is detected as an increase in the *np* signal. Depending on the geometry of the experiment, the ions are either accelerated directly into a microchannel plate detector, as shown in Fig. 7(a), or a set of deflection plates is used to direct the ion beam into the detector, as shown in Fig. 7(b). The ion signal from the detector is amplified by 40 dB and sent to a gated integrator which is set to record the *np*-state signal. A microcomputer, which is also used to control the sweeping of the dc electric field, records the output of the integrator and averages the data over a number of sweeps.

IV. RESULTS

A. Resolved fine-structure components

Due to the fine structure of the *p* states there are actually nine components of the $ns+ns\rightarrow np+(n-1)p$ transition. Figure 8 shows the energy levels of Na which are involved in the resonant collisional energy transfer for $n=17$. Because the two $m_s=\pm\frac{1}{2}$, $m_l=\pm1$ levels of the *p*

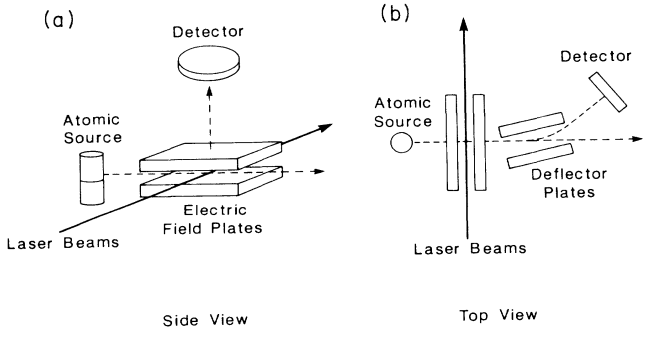

FIG. 7. Experimental apparatus configured so that (a) the electric field is perpendicular to the collisional velocity, and (b) the electric field and collisional velocity are parallel.

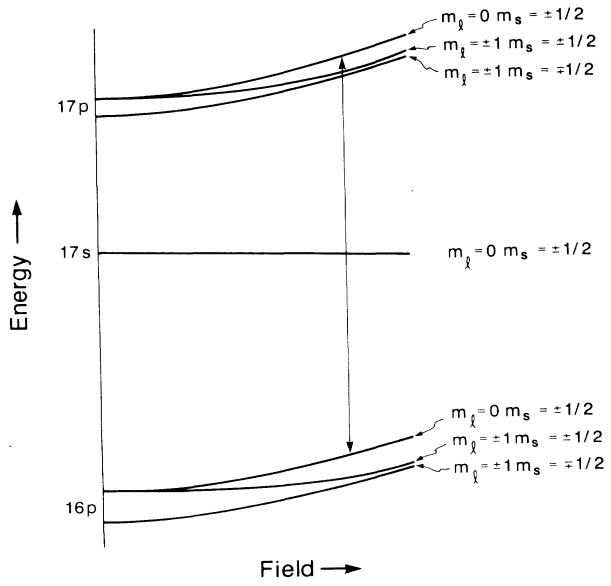

FIG. 8. Energy-level diagram for the transition $17s+17s\rightarrow17p+16p$ in Na.

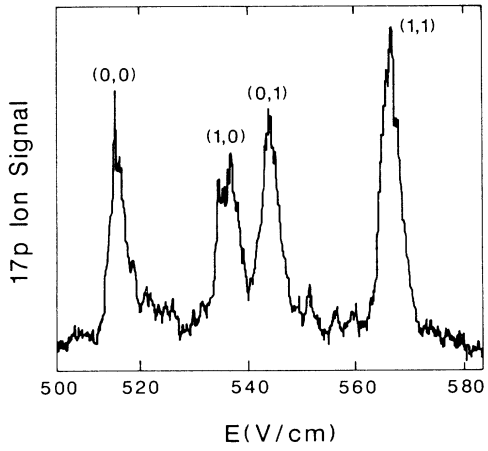

FIG. 9. Previous measurement of the $17s+17s \rightarrow 17p+16p$ transition showing the resolution of the transition into the $m_l=0$ and 1 components. The resulting four components are labeled with the m_l values of the upper and then lower p states.

state are very closely spaced at the electric field strength at which the resonances occur, in previous measurements[1] they were not resolved and only four separate transitions were observed, as shown in Fig. 9. This led to the convention in which the transitions were labeled by the m_l values of the upper and lower p states, so that the four transitions observed were denoted (in order of increasing electric field) (0,0), (1,0), (0,1), and (1,1). (It should be noted that in Ref. 1, the figures are labeled as described above, but the description in the text is inconsistent with this convention.) In the present work, the components of the (1,0), (0,1), and (1,1) transitions are well resolved, as seen in Fig. 10 for $n=16$. As a result, a slightly different labeling convention is needed. In this work, transitions to the $m_l=\pm 1$ states will be labeled with a 1_+ or a 1_-, depending on whether the sign of m_s is the same as or opposite that of m_l. Table I lists the resonant fields for all nine of these components as measured in this experiment for $n=16$–24.

Since the $(1_+,0)$ to $(1_-,0)$ separation is now resolved, it is interesting to compare the n^* scaling of this splitting (where n^* is the effective principal quantum number of the s state) to a simple prediction, obtained in the following manner. Using the $(1_+,0)$ transition as a starting point, it is clear that a small increase in the electric field will bring the $(1_-,0)$ transition into resonance as shown by Fig. 11.

Since the s-state energy is approximately constant for a small change in electric field and the Stark shift of the p states is predominantly quadratic, the $(1_-,0)$ resonance occurs when

$$2\alpha_{np}F\Delta F=\Delta E_{\rm FS}-2\alpha_{(n-1)p}F\Delta F \ ,$$

where F is the electric field at which the $(1_+,0)$ resonance occurs and ΔF is the change in field between the $(1_+,0)$ and $(1_-,0)$ transitions. Furthermore,

$$\Delta E_{\rm FS}=\Delta E_{{\rm FS}_0}\frac{k}{3} \ ,$$

where $\Delta E_{{\rm FS}_0}$ is the zero-field fine-structure interval and k is the amount of p character in the nominally p state. Thus

$$\Delta F\simeq\Delta E_{{\rm FS}_0}\frac{k}{12\alpha F} \ .$$

It is well known that $\Delta E_{{\rm FS}_0}$ scales as $(n^*)^{-3}$ and that the polarizability $\alpha\sim(n^*)^7$. If we assume that the n^* dependence of $k(F)$ is negligible, and if we use Safinya *et al.*'s[1] empirical result that $F\sim(n^*)^{5.3}$, we arrive at the scaling law

$$\Delta F\sim(n^*)^{-4.7} \ . \tag{7}$$

A similar value for the exponent can be derived using a numerical approach. The energy levels of Na near the resonances for $17s$ and $24s$ were calculated using the technique described by Zimmerman *et al.*[9] for diagonalizing the energy matrix. The $(1_+,0)$ to $(1_-,0)$ field intervals found by comparing the ns-np spacing with the $ns-(n-1)p$ spacing were least-squares fit to a power law and yielded the result

$$\Delta F\sim(n^*)^{-4.58} \ . \tag{8}$$

TABLE I. Experimental electric field values at which resonances occur.

State	Resonance field (V/cm) (0,0)	$(1_+,0)$	$(1_-,0)$
16s	744.2(5)	770.3(5)	773.6(5)
17s	519.0(3)	538.0(3)	540.3(3)
18s	371.5(3)	385.6(3)	387.3(3)
19s	271.3(2)	281.9(2)	283.2(2)
20s	201.8(2)	209.8(2)	210.7(2)
21s	152.5(2)	158.7(2)	159.4(2)
22s	117.7(2)	122.6(2)	123.2(2)
23s	90.2(2)	94.0(2)	94.6(2)
24s	70.9(2)	94.0(2)	74.4(2)
	$(0,1_+)$	$(0,1_-)$	$(1_+,1_+)$
16s	782.7(5)	784.6(5)	811.6(5)
17s	546.6(3)	548.0(3)	567.7(3)
18s	391.6(3)	392.8(3)	407.5(3)
19s	286.2(2)	287.1(2)	298.2(3)
20s	213.4(3)	214.0(3)	222.7(4)[b]
21s	161.6(2)	162.0(2)	168.3(4)[b]
22s	124.4(4)[a]		129.1(4)[b]
23s	95.6(4)[a]		100.4(4)[b]
24s	75.0(3)[a]		78.9(3)[b]
	$(1_-,1_+)$	$(1_+,1_-)$	$(1_-,1_-)$
16s	813.5(6)	814.6(6)	816.5(6)
17s	569.2(4)	569.8(3)	571.3(3)
18s	408.6(3)	409.2(3)	410.2(3)
19s	299.1(3)	299.5(3)	300.3(3)

[a]Center of unresolved $(0,1_+)$, $(0,1_-)$ doublet.
[b]Center of unresolved (1,1) resonances.

Experimental measurements were made for the same $(1_+,0)$ to $(1_-,0)$ intervals. The results, shown in Table II, agree with the calculated values to within the experimental uncertainty, and a least-squares fit of these data gives

$$\Delta F \sim (n^*)^{-4.76(16)} , \tag{9}$$

which is in good agreement with both the predicted and calculated values.

B. Relative cross sections for v∥E and v⊥E

In order to obtain high-resolution data, electric field plates were used to create a homogeneous static electric field. Thus, to study the two cases of **v∥E** and **v⊥E**, it was necessary to use two different sets of field plates with different ion or electron collection paths, as described above. As a result, it was difficult to compare the relative cross sections in the two cases. To overcome this difficulty, another apparatus was used in which the direction of the static electric field could be quickly changed. Since the details of this apparatus are given elsewhere,[10] only a brief description follows.

In this part of the experiment, the electric fields were created by a set of four parallel wires. The pulsed ionization field was created by a voltage applied to the lower two wires, and it accelerated the ions in the same direc-

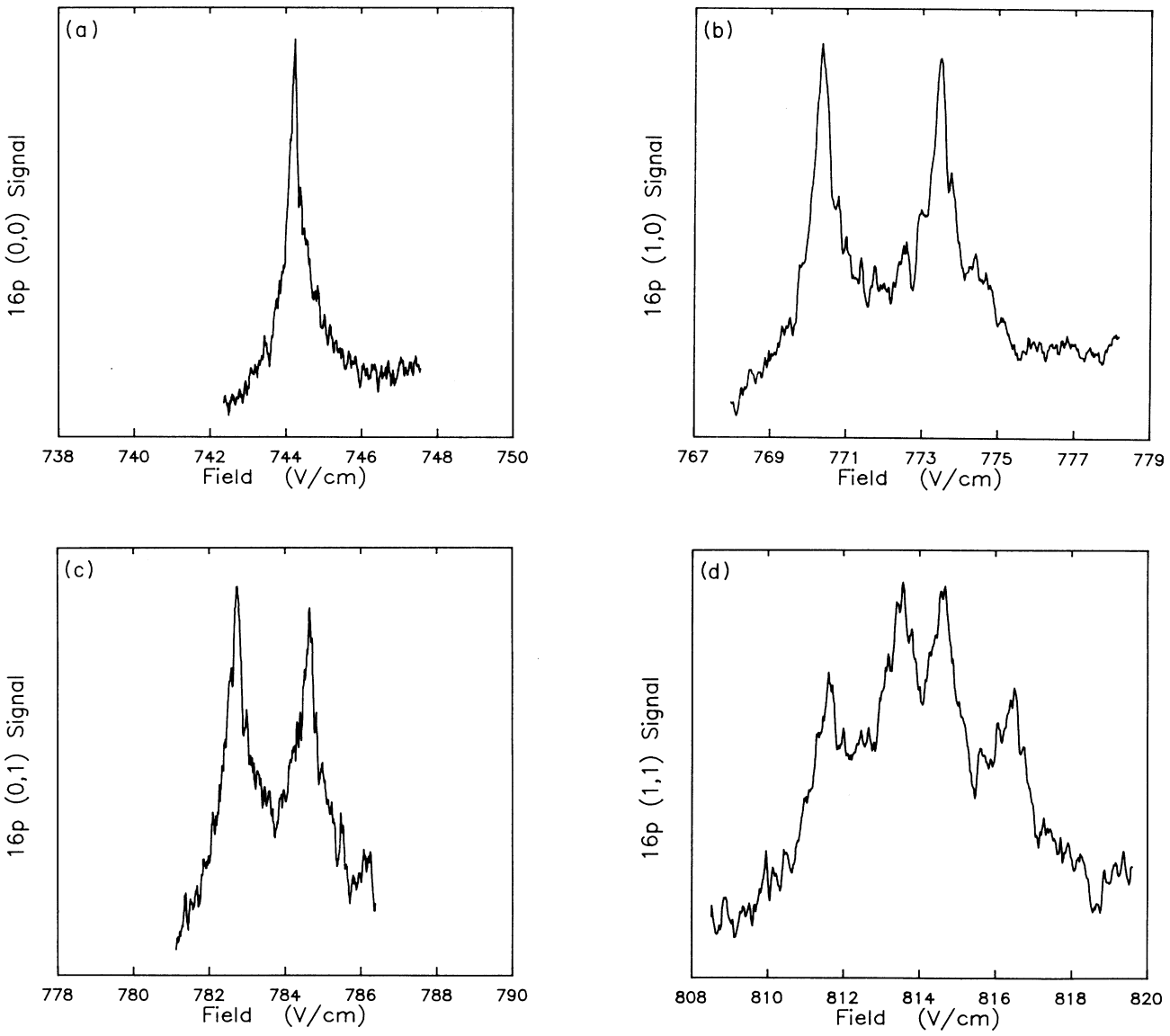

FIG. 10. Current measurements of the $16s+16s \rightarrow 16p+15p$ resonance with **v⊥E** showing the resolution of the fine structure of the p states: (a) the (0,0) transition, (b) the $(1_+,0)$ and $(1_-,0)$ transitions, (c) the $(0,1_+)$ and $(0,1_-)$ transitions, and (d) the $(1_\pm,1_\pm)$ transitions. The labeling scheme is the same as in Fig. 8, except that the $\pm$ subscript indicates whether m_s has the same or opposite sign as m_l for a particular state.

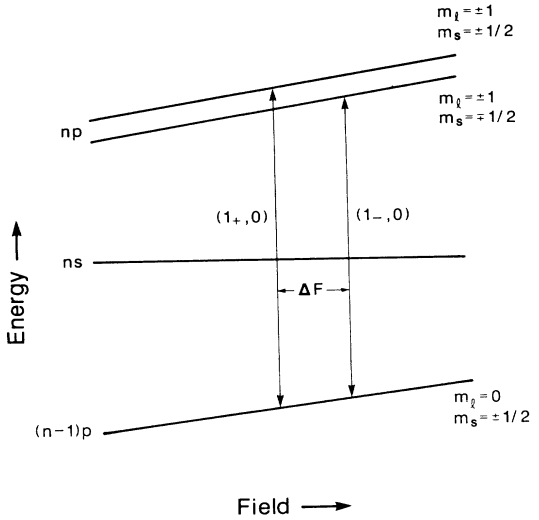

FIG. 11. Detail of the energy levels of Na in an electric field near the $(1_+,0)$ and $(1_-,0)$ resonances. The resonances are labeled as in Fig. 9, and ΔF is the separation in electric field between the $(1_+,0)$ and $(1_-,0)$ transitions.

tion regardless of the orientation of the static electric field. The static field was created by applying a voltage to either the lower two wires or one lower wire and one upper wire. With this arrangement, selection of the angle between **v** and **E** could be made in a few seconds, ensuring that the data for each case were taken under similar circumstances. In particular, the atomic density of the sodium beam, which drifts slowly in time, was nearly the same for two consecutive scans.

Since an analytical solution for the electric field produced by the wires cannot be found, a relaxation technique was used to calculate the electric field homogeneity for this apparatus. It was found that in the interaction region, the field homogeneity was slightly better than one part in 10^2. Thus, although details of the line shape and fine-structure intervals could not be measured with this appartus, the homogeneity was sufficient for low-resolution comparisons of the collision cross sections. When such measurements were made for $n = 26$, it was found that the cross sections for the two geometric configurations were indeed on the same order of magnitude. In particular, the cross section for **v**||**E** was found to be approximately 80% of that for **v**⊥**E**. This is in fair agreement with the calculated cross sections, since the calculation for the **v**||**E** cross section did not involve an average over the angle θ.

TABLE II. Experimental and calculated values of the $(1_+,0)$ to $(1_-,0)$ field interval.

n (of s)	ΔF_{expt} (V/cm)	ΔF_{calc} (V/cm)
16	3.22(8)	
17	2.29(5)	2.24
18	1.70(7)	1.68
19	1.29(6)	1.29
20	0.96(8)	1.00
21	0.68(10)	0.78
22	0.57(11)	0.64
23	0.53(10)	0.51
24	0.39(10)	0.43

C. Line shapes for v||E and v⊥E

Using the experimental geometry of Fig. 7(a) we have carefully studied the line shape of the (0,0) resonance for **v**⊥**E**, with the result shown in Fig. 12(b). As shown by Fig. 12(b), the result is a nearly symmetric Lorentzian line shape, in reasonable accord with the theoretical prediction, as depicted in Fig. 2(b). For reasons given below we are reasonably confident that there is no structure in the line shape obscured by instrumental effects.

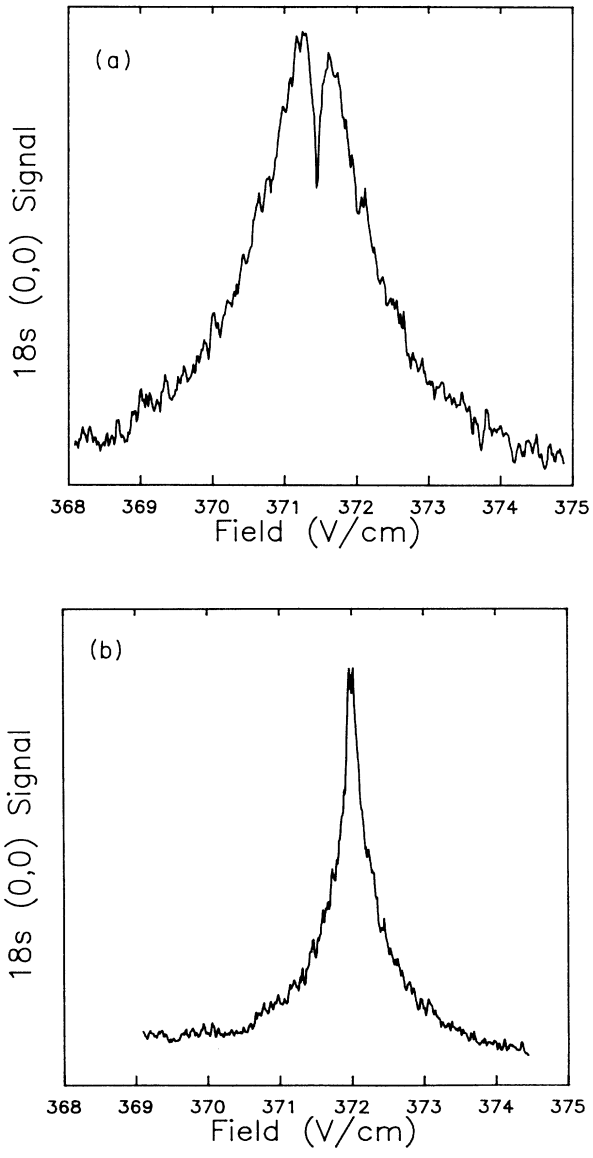

FIG. 12. Experimental measurements of the 18s (0,0) resonance for (a) **v**||**E** and (b) **v**⊥**E**. Note the definite dip near the center of the resonance in (a), as well as the slight asymmetry, both of which agree with the numerical predictions.

The results of the experiments with $\mathbf{v}\|\mathbf{E}$ are strikingly different. These experiments, carried out with the experimental configuration of Fig. 7(b), yield a very clear double-peaked line shape, with a pronounced dip in the center, as predicted by the theoretical calculations and shown in Fig. 2(a), for example. Theoretically the dip in the center of the line shape should go to zero. There are, however, several experimental realities which prevent this from happening.

First, the feature predicted in Fig. 2 has a width of 5×10^{-4} times the electric field at which it occurs, whereas previous measurements indicate that the electric field used has a homogeneity of 1 part in 10^4. The presence of a background of sodium vapor atoms with randomly directed velocities adds a $\mathbf{v}\perp\mathbf{E}$ signal which has no dip in the center. Finally, the imperfect collimation of the sodium beam also contributes a nonvanishing background.

In Fig. 12(a) there is also a clear asymmetry; the peak on the low-field side of the dip is larger than the peak on the high-field side, just as the calculations in Fig. 6 predict. Since the asymmetry is predicted only when the permanent dipole moments are taken into account, we interpret the asymmetry as clear evidence of the effect of the permanent dipole moments.

It is also clear that the experimental width of the $\mathbf{v}\perp\mathbf{E}$ signal is less than half of that of the $\mathbf{v}\|\mathbf{E}$ signal. Again, this is consistent with the calculations shown in Fig. 5 in which the full width at half maximum (FWHM) of the $\mathbf{v}\|\mathbf{E}$ cross section is nearly twice the FWHM of the $\mathbf{v}\perp\mathbf{E}$ cross section. Also, day-to-day variations in oven temperatures and other experimental parameters could easily account for the fact that the experimental width of the $\mathbf{v}\perp\mathbf{E}$ cross section is somewhat narrower than expected based on the calculations.

Finally, it might be noted that experimentally the $\mathbf{v}\|\mathbf{E}$ peak is shifted to a slightly higher electric field relative to the $\mathbf{v}\|\mathbf{E}$ peak. Although a slight shift in the same direction can be seen in the calculated cross sections, it must be remembered that the $\mathbf{v}\perp\mathbf{E}$ cross section was calculated for only one value of θ; thus the experimental shift cannot be interpreted as verifying this aspect of the calculations. Instead, we interpret the observed shift as a possible combination of an authentic shift in the resonance field and experimental uncertainty arising from the fact that different sets of field plates were used for the two geometries. In principle, it is possible to calibrate the electric field more exactly using an anticrossing measurement technique.[11] However, we felt that the small magnitude of both the predicted and observed shifts did not warrant this substantial increase in the complexity of the experiment.

V. CONCLUSIONS

A careful examination of the theory of resonant dipole-dipole collisional energy transfer reveals important differences between $\mathbf{v}\|\mathbf{E}$ and $\mathbf{v}\perp\mathbf{E}$. In particular, in the former case, the collision cross section vanishes at exact resonance due to destructive interference in the transition amplitudes during different parts of the collision. Rather surprisingly, the large permanent dipole moments have only a small effect, contributing a small shift and asymmetry to the line shape.

Both the above predictions have been verified experimentally using higher-resolution experimental configurations which allow the study of $\mathbf{v}\|\mathbf{E}$ and $\mathbf{v}\perp\mathbf{E}$. Additionally, the higher resolution made it possible to resolve the previously unresolved spin-orbit structure in the collisional resonances.

ACKNOWLEDGMENT

This research has been supported by the U.S. Air Force Office of Scientific Research under Grant No. AFOSR-87-0007-B.

*Permanent address: Sachs-Freeman Assoc., 1401 McCormick Drive, Landover, MD 20785.

[1]K. A. Safinya, J. F. Delpech, F. Gounand, W. Sandner, and T. F. Gallagher, Phys. Rev. Lett. **47**, 405 (1981); T. F. Gallagher, K. A. Safinya, F. Gounand, J. F. Delpech, W. Sander, and R. Kachru, Phys. Rev. A **25**, 1905 (1976).

[2]R. Kachru, N. H. Tran, and T. F. Gallagher, Phys. Rev. Lett. **49**, 191 (1982).

[3]P. Pillet, R. Kachru, N. H. Tran, W. W. Smith, and T. F. Gallagher, Phys. Rev. Lett. **50**, 1763 (1983).

[4]N. F. Ramsey, *Molecular Beams* (Oxford University Press, London, 1956).

[5]R. M. Herman, Phys. Rev. Lett. **42**, 1206 (1979).

[6]E. Fiordilino, G. Ferrante, and B. M. Smirnov, Phys. Rev. A **35**, 3674 (1987).

[7]D. R. Hartree, *Numerical Analysis* (Oxford University Press, London, 1958).

[8]T. F. Gallagher, L. M. Humphrey, W. E. Cooke, R. M. Hill, and S. A. Edelstein, Phys. Rev. A **16**, 1098 (1977).

[9]M. L. Zimmerman, M. G. Littman, M. M. Kash, and D. Kleppner, Phys. Rev. A **20**, 2251 (1979).

[10]D. S. Thomson, M. S. thesis, University of Virginia, 1988 (unpublished).

[11]R. C. Stoneman, G. Janik, and T. F. Gallagher, Phys. Rev. A **34**, 2952 (1986).